IEEE Photonics Journal
An IEEE Photonics Society Publication

Open Access

Restoration of Sparse Aperture Images Using Spatial Modulation Diversity Technology Based on a Binocular Telescope Testbed

Volume 9, Number 3, June 2017

Zongliang Xie
Haotong Ma
Bo Qi
Ge Ren
Jianliang Shi
Li Dong
Yufeng Tan
Zhipeng Wang
Xiaojun He

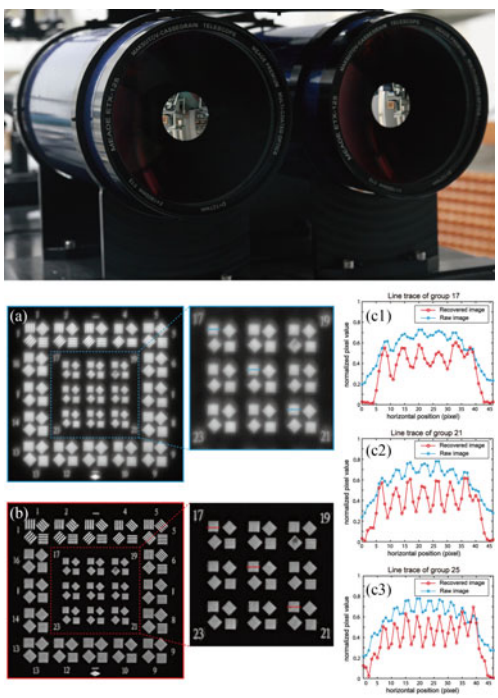

DOI: 10.1109/JPHOT.2017.2700939
1943-0655

IEEE photonics SOCIETY
IEEE

Restoration of Sparse Aperture Images Using Spatial Modulation Diversity Technology Based on a Binocular Telescope Testbed

Zongliang Xie,[1,2,3] Haotong Ma,[1,2,4] Bo Qi,[1,2] Ge Ren,[1,2] Jianliang Shi,[1,2] Li Dong,[1,2,3] Yufeng Tan,[1,2,3] Zhipeng Wang,[1,2,3] and Xiaojun He[1,2,3]

[1]Key Laboratory of Optical Engineering, Chinese Academy of Sciences, Chengdu 610209, China
[2]Institute of Optics and Electronics, Chinese Academy of Sciences, Chengdu 610209, China
[3]University of Chinese Academy of Sciences, Beijing 100039, China
[4]College of Opto-Electronic Science and Engineering, National University of Defense Technology, Changsha 410073, China

DOI:10.1109/JPHOT.2017.2700939

Manuscript received March 29, 2017; revised April 26, 2017; accepted April 29, 2017. Date of publication May 16, 2017; date of current version June 1, 2017. This work was supported by the National Natural Science Foundation of China under Grant 61205144. Corresponding authors: Zongliang Xie and Haotong Ma (e-mail: zongliang.xie@yahoo.com; mahaotong@163.com).

Abstract: In this paper, our recently developed spatial modulation diversity technology (SMDT) is first used to correct the blurring and restore the lost midband contrast of synthetic images based upon an actual sparsely filled aperture system, specifically a binocular telescope testbed consisting of two horizontally arranged collector telescopes with 127 mm diameter. Synthetic images are obtained with the testbed cophased by an optimization algorithm. Diversity images are generated by using electronic shutter to modulate the transmittance of each subaperture, alternately. We capture two independent datasets corresponding to different objects regarded as the reference of each other. Then an improved algorithm of SMDT for real sparse aperture systems is proposed to restore the synthetic imagery by processing the datasets. The experimental results that the reconstructed images present high quality and contrast and that the repeatable wavefront measurements show a good agreement demonstrate the availability of SMDT for image restoration in actual multiaperture systems.

Index Terms: Spatial modulation diversity technology, binocular telescope testbed, image restoration.

1. Introduction

With modern technology developing, astronomical space observation needs the apertures of optical imaging systems to be large enough to meet the requirement of the desired high resolution. Unfortunately, the large aperture would bring big challenges to the fabrication and cost with the mass and volume of systems increasing undesirably. In this case, optical sparse aperture imaging has grown out of the quest for solving the contradiction between higher angular resolution and large aperture telescopes [1]. By using several co-phased small sub-apertures to synthesize images, sparse aperture systems can achieve the same resolution as a fully-filled aperture with a smaller

overall light collection area. However, sparse arrangement of sub-apertures also trades off many midband spatial frequencies, causing the corresponding modulation transfer function (MTF) greatly attenuated. As a result, the raw images directly collected by sparse aperture systems are poor, suffering from significant blurring and loss of contrast [2].

Many approaches have been proposed in literature to address the problem. Specifically, a holography-based aperture synthesis using multi-transmitter to compensate for the lost contrast has been demonstrated [3]. As a coherent imaging method, it requires complex light paths and is easy to be affected by the inevitable speckle noise. Alternately, Stokes *et al.* concentrated on the configuration of aperture array to search for the possibility of increasing the midband contrast. They have given a successful example by increasing the diameters of the middle set of sub-apertures of Golay-9 [4]. Also, image restoration method is another powerful tool for midband contrast improvement. Blind deconvolution for traditional single-aperture images has been widely researched for many years and many algorithms that can estimate the point spread function (PSF) during the deconvolution process by imposing regularized terms or sparsity constraints have been proposed [5]–[6]. Nevertheless, the validity of these algorithms for estimating the PSF of a sparse-aperture system, which is an interference pattern rather than an Airy disk, has not been demonstrated up to now. Some deconvolution algorithms [2], [7]–[9] handled successfully in simulated sparse-aperture systems with pupil-masks need the PSFs to be known. The PSF can be easily computed according to the pupil arrangement in pupil-mask experiment, but acquiring the correct PSF by this way in practical sparse-aperture systems is a challenging problem due to the unknown aberrations of sub-aperture systems. Also, it is difficult for the experimentally captured PSF to match the actual PSF because of the inevitable influence of noise, which may lead to the failure in image restoration [7].

Phase diversity is another well-known method of image restoration, which can estimate the PSF adaptively by using diversity images. Gonsalves first proposed phase diversity for wavefront sensing of single aperture systems [10], and it has been studied and developed widely for both single and multiple aperture systems [11]–[17]. Conventional phase diversity using defocus diversity has been used in Star-9 synthetic system [15]. Some researchers modified the conventional method and proposed different diversities. Chromatic phase diversity using 3 spectral channels has been proposed to co-phase sparse-aperture systems [16]. Alternatively, a sub-aperture piston phase diversity has also been reported to restore images for sparse aperture systems [17]. Recently we have developed a new method of phase diversity for synthetic aperture imaging, termed spatial modulation diversity technology (SMDT), which has shown the potential to restore the image with adaptively estimated PSF [18]. Differing from the existing focus, sub-aperture piston, and wavelength diversity, SMDT uses simple electronic shutter to generate spatial diversity without defocusing optics, other spectral channels and high precision actuators used, which compacts the system and reduces the complexity and cost. It is also absolutely different from another form of aperture diversity, termed transverse translation diversity (TTD) [19]. TTD can extract the wavefront of a single-aperture imaging system using phase retrieval algorithm from a series of raw images generated by a scanning sub-aperture, while SMDT is aimed at jointly realizing wavefront sensing and image restoration for sparse-aperture systems by using phase diversity algorithm to process diversity images yielded by controlling the transmittance of each sub-aperture with electrical shutters. Nevertheless, it is also only demonstrated in a proof-of-principle experiment using pupil-mask to simulate a sparse aperture system without the influence of sub-aperture aberrations and many errors inevitably existing in a practical system, such as co-phasing error, magnification error, defocus error and pupil mapping error. It is necessary to test the performance of SMDT in a practical system suffering such sub-aperture aberrations and inevitable system errors.

In this paper, we first demonstrate this approach for image restoration in an actual multi-aperture system. A binocular telescope testbed consisting of two horizontally arranged collector telescopes with 127 mm diameter has been built in our laboratory. Synthetic images using different resolution test charts with horizontal resolution obviously improved are acquired after the two sub-apertures are co-phased by using an optimization algorithm to control the specially designed actuator. Then we capture other single aperture images as diversity datasets by switching off each electronic

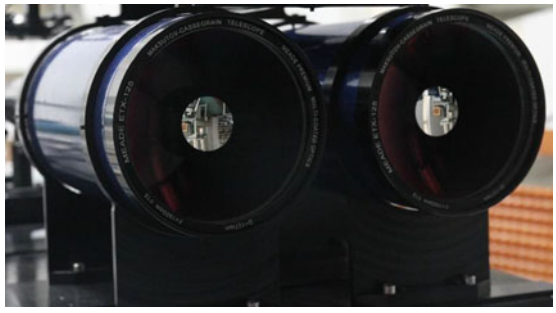

Fig. 1. Front view of the binocular telescope testbed.

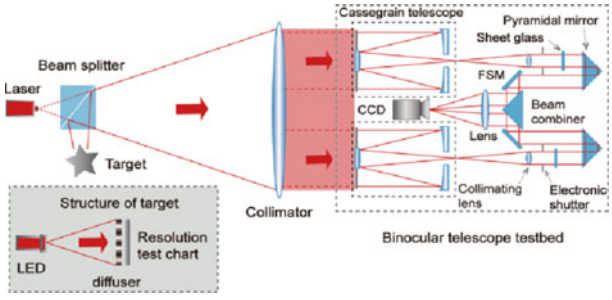

Fig. 2. The optical configuration of the binocular telescope testbed and the collimated scene projector. FSM: fast steering mirror.

shutter attached to sub-apertures, alternately. Restored synthetic images showing less blurring and high contrast can be obtained by using an improved SPGD algorithm to process the raw images. The two independent data sets can be the reference of each other and a good agreement between the repeatable wavefront measurements is also presented. Note that the algorithm used here for real sparse aperture systems is also different from our previous one, because it needs to consider both the aberrations of imaging beams and sub-apertures while only modeling the former is enough in previous pupil-mask experiment [18].

This paper is structured as follows. In Section 2, the design of the binocular telescope testbed is introduced and the direct experimental results are presented. Section 3 describes the improved algorithm of image restoration associated with the testbed. Section 4 shows the reconstructed results. Finally, the conclusions are given in Section 5.

2. The Binocular Telescope Testbed

To verify the performance of SMDT in restoration of images generated directly by an actual sparse telescope system, we have established a binocular telescope testbed in our laboratory, of which a front view is shown in Fig. 1. The testbed consists of two Maksutov-Cassegrain telescopes, each with a diameter of 127 mm and focal length of 1900 mm (Meade's product, ETX-125). They are arranged horizontally in a center-to-center distance of 180 mm.

2.1. Experimental Setup

Fig. 2 shows the schematic of the optical components of the testbed and how the beams are combined. A collimator with a focal length of 3000 mm is used here as a scene projector. We first use a red point source as the scene to calibrate the optical scheme and co-phase the two sub-telescopes. Then the scene is changed to an extended object uniformly illuminated by a red LED light source with a diffuser inserted into its illumination path. To show an intuitive resolution improvement, we choose a resolution test chart as the target. We note that,

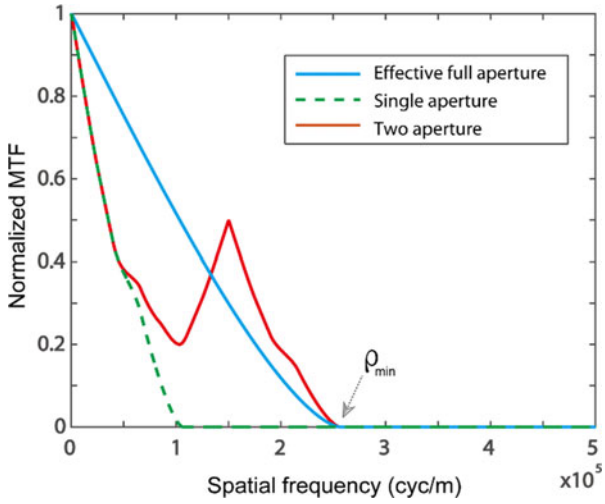

Fig. 3. The MTF profiles along horizontal axis of the single aperture, two aperture and horizontal effective full aperture systems.

centering on the image restoration, this paper doesn't consider 2π ambiguity of optical path, while as an important issue, co-phasing the testbed using a white-point source needs our future investigation.

For one aperture in the testbed as shown in Fig. 2, the Maksutov-Cassegrain telescope and a collimating lens with a focal length of 180 mm constitute an afocal telescope to collect light coming from the collimated scene projector, behind which an electronic shutter is located to control the beam travel. The collected light permitted to pass then propagates through a sheet glass mounted on a high-precision rotation stage, which is designed to realize precision path length adjustment. Following the sheet glass, a pyramidal mirror, which is mounted on a motorized translation stage to adjust optical path length coarsely, sends the light onto a fast steering mirror (FSM), which is active in tip-tilt alignment. Then an outwardly reflective pyramidal mirror serving as a beam combiner injects the beam reflected from the FSM onto an imaging lens. The beam collected by the other aperture goes through the same travel described above. Finally, the imaging lens with a focal length of 180 mm synthesize the two beams onto a CCD camera (Daheng Image's product, MER-1070-10GM/GC) with a 3840 $\times$ 2748 array of 1.67 μm pixel pitch.

To achieve a synthetic image successfully, there is a well-known golden rule [20] needed to be obeyed, which requires the output pupil of the testbed to be a scaled replica of its entrance pupil. In our testbed, the beam combiner is controlled by a high-precision motorized translation stage. Moving the combiner prism along with the axis vertical to the baseline of the binocular telescope makes the two incidence beams incident on different positions of the combiner reflective surface, permitting their distance to be adjusted with the emergent angles keeping unchanged. In this way, we realize the control of the pupil mapping error.

2.2. MTF Analysis

It is necessary to examine the theoretical imaging performance of the testbed. By describing the capability of an incoherent imaging system for transfering object spatial frequency to an image [21], the MTF can achieve superior quantification of image quality, with respect to single-number measures, such as Strehl. As a direction dependant in the spatial frequency plane, it also directly gives intuitive information about resolution and image contrast. For the advantages, we choose the MTF to analyze the theoretical imaging performance. Fig. 3 depicts the MTF profile of the testbed in horizontal direction, and the ones of the horizontal effective full aperture and single aperture systems are also given as a contrast, respectively.

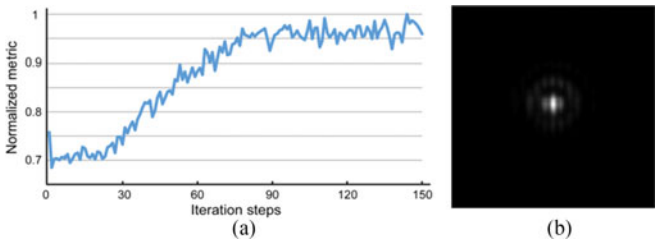

Fig. 4. Co-phased results using SPGD optimization algorithm: (a) the optimization evolution of the SPGD algorithm; (b) the final co-phased PSF.

Based on the presented MTFs, the imaging ability of the testbed in resolution and contrast can be predicted. First, the horizontal MTF profile of the testbed shows larger spatial frequency cutoff compared with that of the single aperture system, indicating that higher resolution in horizontal direction is available. The diameter D_{eff} of an effective full aperture system in horizontal direction having the same horizontal resolution as the binocular system can be calculated using the following equation with the numerically found spatial frequency cutoff ρ_{min} [4].

$$D_{\text{eff}} = \rho_{\text{min}} \lambda f \tag{1}$$

where λ is the imaging wavelength, and f is the equivalent focal length. Given a wavelength of 632 nm and a calculated horizontal effective diameter of 307 mm, it is easy to obtain the horizontal theoretical resolvable spot angle of 2.51 urad using the Rayleigh criteria, while that of the single system is 6.07 urad. Second, it is apparent that there is a deep gap between the main lobe and side lobe in the horizontal MTF profile of the binocular testbed, meaning lower energy at the midband spatial frequency along the horizontal axis than that of the effective full-filled aperture system. Thus the images formed by the testbed have poor contrast.

2.3. Experimental Results

After analyzing the imaging performance of the testbed in theory, we present the experimental results. To acquire a successfully synthetic image, the two sub-apertures need to be co-phased within a fraction of the wavelength where the optimal performance of the sparse aperture system can be achieved [9], [22] and such a minor phase difference has little impact on SMDT. If the phase difference exceeded a fraction of the wavelength, the mid-frequency would lose more energy, easily leading that the information at the corresponding midband frequencies can't be recovered by SMDT. In this paper, we use an automatic closed-loop mode with the stochastic parallel gradient descent (SPGD) algorithm to co-phase the system. The phasing issue is considered as an optimization problem here, with a sharpness metric defined as a function of the control parameters [22], [23]. Muller and Buffington have demonstrated that some metrics could achieve their maximum value only without aberrations [24]. Here, we use one of their defined sharpness metrics, expressed as

$$E = \sum_{x} \sum_{y} I^2(x, y) \tag{2}$$

where x, y denote coordinates in the image plane and $I(x, y)$ is the captured PSF. Then the SPGD algorithm, whose details can be referred to Ref. [23], is used to maximize the sharpness function by controlling the actuators, generating the co-phasing results shown as Fig. 4. Fig. 4(a) presents the evolution of the algorithm, from which it can be seen that its maximum value is achieved after about 80 iterations, and Fig. 4(b) shows the final co-phased PSF.

After our co-phasing the two telescopes, the object scene is changed to an A4 resolution test chart. Fig. 4 presents the direct experimental imaging results. The synthetic image is shown in Fig. 5(c1), while the left single aperture image is shown in Fig. 5(a1) and the right one is shown in Fig. 5(b1) as reference. It can be recognized by carefully viewing that the synthetic image presents higher resolution in the horizontal direction compared with both single aperture images

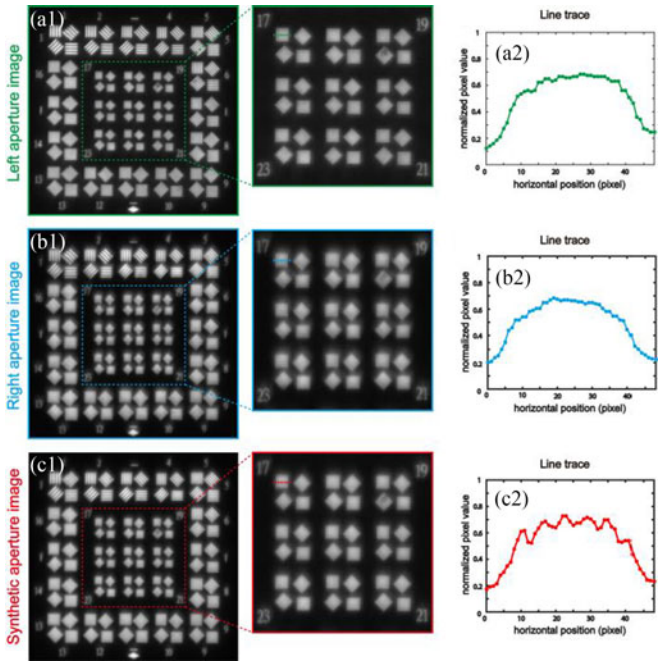

Fig. 5. Imaging results of the binocular telescope testbed with the A4 resolution chart. (a1) the image formed by the single left aperture; (b1) the image formed by the single right aperture; (c1) the synthetic image formed by the co-phased two aperture; (a2)–(c2) the line traces of vertical bars of group 17 corresponding to (a1)–(c1), respectively.

from the amplified region. The difficult observation of resolution improvement is mainly caused by the loss of contrast. We take the line traces of vertical bars of group 17 to show the clear resolution enhancement. The line traces of single aperture images shown as Fig. 5(a2) and 5(b2) indicate unsolved results with flat variation in the bar region, matching the fact that the neighboring bar distance of 16.82 um corresponding to a resolution spot angle of 5.6 urad is beyond the resolvable limitation of a single aperture given in 2.2. Luckily, our binocular telescope having the horizontal resolvable spot angle of 2.51 urad can distinguish these vertical bars. As presented in Fig. 5(c2), the plot obviously shows a periodic fluctuation, indicating that the 6 vertical bars are resolved, while the small difference between the peak and valley implies the low contrast.

As theoretically predicted in Section 2.2, the directly synthetic image has higher horizontal resolution but lower contrast. In this situation, a method of image restoration is necessary to improve the sharpness and contrast of the sparse aperture image.

3. Algorithm of SMDT Associated with The Testbed

In this section, we introduce the principle of our processing algorithm associated with the testbed and how it works. The intensity images captured by CCD detector can be represented as

$$d_k(x) = o(x) \otimes h_k(x) + n_k(x) \tag{3}$$

where $d_k(x)$ is the recorded image, the subscript k stands for the kth spatial modulation, $o(x)$ is the ideal image intensity, $h_k(x)$ represents the point spread function (PSF) of the system with the kth modulation, $n_k(x)$ is the corresponding additive noise, $\otimes$ denotes a convolution, and x is a 2D vector in image plane. The spatial modulation is realized by using electronic shutter to control the transmittance of each sub-aperture in sequence. Specifically in our testbed, the 1st modulation is performed by opening the two sub-apertures, the 2nd one is by turning off the right sub-aperture, and the 3rd one is by turning off the left sub-aperture. According to the imaging theory [21], the intensity PSF can be associated with the generalized pupil function $P_k(u)$ generated by the kth

modulation, which can be modeled as

$$P_k(u) = \begin{cases} p_{left}(u)\exp(i\varphi_{left}) + p_{right}(u)\exp(i\varphi_{right}) & k = 1 \\ p_{left}(u)\exp(i\varphi_{left}) & k = 2 \\ p_{right}(u)\exp(i\varphi_{right}) & k = 3 \end{cases} \tag{4}$$

where $p_{left}(u)$ and $p_{right}(u)$ are the binary pupil functions of the left sub-aperture and right sub-aperture, respectively, φ_{left} and φ_{right} are their corresponding aberrations. When used in the pupil mask experiment [18], the algorithm only needs to consider the global aberration of the imaging beam, which can describe the phase errors loaded by the imaging lens and transmission medium. However, for an actual sparse aperture system like our binocular telescope, besides the imaging beam distortion, the aberrations of sub-aperture system also need to be taken into account to estimate an accurate PSF. Here we use two independent phase distributions to denote the wavefront, which are characterized by a combination of a series of Zernike polynomials, as follows

$$\begin{cases} \varphi_{left} = \exp[i\sum_{n=1}^{N}\alpha_n Z_n(u)] \\ \varphi_{right} = \exp[i\sum_{n=4}^{N}\beta_n Z_n(u)] \end{cases} \tag{5}$$

where $Z_n(u)$ is the nth order Zernike polynomial, α_n, β_n and ν_n are the Zernike expansion coefficients regarded as the control parameters, N is the order of Zernike polynomials, and u is a 2D vector in pupil plane. To denote the piston and x and y tilt between the two sub-apertures, the aberrations of the left aperture contains the first 3 Zernike polynomials while the right aperture is taken as the reference aperture with them excluded.

Following the models above, the PSF is described as a function with respect to pupil functions known as a priori knowledge and Zernike coefficients needed to be optimized. We then give a following optimization metric in Fourier domain based on Gaussian log-likelihood framework

$$E(f, \alpha, \beta, \nu) = \sum_{k=1}^{3}\sum_{f}[D_k(f) - O(f)\cdot H_k(f)]^2 \tag{6}$$

where f is a 2D vector in Fourier domain, $D_k(f)$, $O(f)$ and $H_k(f)$ are 2D Fourier transforms of $d_k(x)$, $o(x)$ and $h_k(x)$. Following the previous work [10], [11], the metric function of (5) can be simplified as:

$$E(f, \alpha, \beta, \nu) = \sum_{f}\sum_{k=1}^{3}|D_k(f)|^2 - \sum_{f}\frac{\left|\sum_{k=1}^{3} D_k(f)H_k^*(f)\right|^2}{\sum_{k=1}^{K}|H_k^*(f)|^2 + \gamma} \tag{7}$$

where $H_k^*(f)$ is the conjugate complex of $H_k(f)$, and γ is a nonnegative regularization parameter. We use stochastic parallel gradient descent algorithm, which can achieve the maximum convergence speed if Zernike polynomials are chosen as a set of influence functions [25], to minimize the metric above with the PSF being estimated adaptively. The details of how algorithm works can be referred in our previous paper [18]. Finally, the reconstructed image can be obtained by using the following equation

$$O(f) = \frac{\sum_{k=1}^{3} D_k(f)H_k^*(f)}{\sum_{k=1}^{3}|H_k(f)|^2 + \gamma} \tag{8}$$

where γ is selected to provide a pleasing image as used in Ref. [9]. Such an unregularized operation is enough due to the captured images shown as Fig. 5 with relatively high signal to noise radio. Here we concentrate on the experimental demonstration of SMDT for image restoration in practical sparse aperture systems with less emphasis on the impact of noise. Also, the impact of the noise on SMDT is an interesting and important issue. To deal with seriously noisy images, an improved SMDT algorithm incorporating more robust Wiener filter with estimation of power spectra [26]–[27] might be helpful, which needs our further investigation.

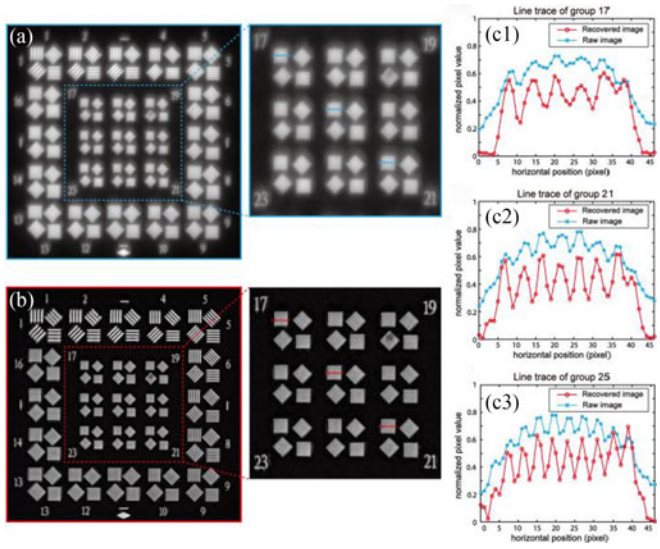

Fig. 6. Comparison of the raw synthetic image (a) and the reconstructed image (b) using SMDT with the A4 resolution test chart; (c1)–(c3) vertical bar line traces of group 17, 21 and 25 of (a) and (b), respectively.

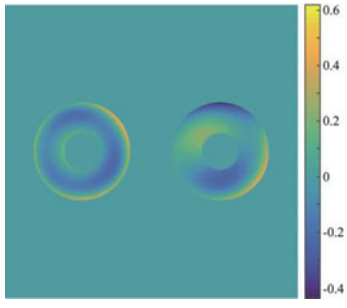

Fig. 7. The recovered wavefront of two sub-apertures using the data set of the A4 resolution test chart.

4. Reconstructed Results

To improve the sharpness and contrast of the synthetic image, we begin our restoration procedure by employing the proposed algorithm to process the raw images and obtain the reconstructed results. Here a detailed experimental analysis is presented as following 3 aspects to validate the effectiveness of SMDT for image restoration in real sparse aperture systems.

First, the recovered image is compared with the raw image. Fig. 6(a) shows the raw synthetic image for comparison and Fig. 6(b) presents the reconstructed one. It is obvious that the sharpness and contrast of the recovery have been greatly improved. In the corresponding amplified area, more sharp texture is presented and more details, especially the group ofhorizontal resolution, are easier to resolve. To give a more explicit sharpness and contrast enhancement, the vertical barline traces of group 17, 21 and 25 are plotted as examples in Figs. 6(c1)–(c3). It can be easily found that more peaks and valleys in recovery line traces are appeared indicating more bars are recovered from blurring, and that the differences between the peaks and valleys become larger demonstrating the contrast improvement. The generated wavefront of the two sub-apertures with tip, tilt and defocus removed is shown as Fig. 7, exhibiting dominate spherical aberration in left pupil and coma in right pupil.

Second, to verify SMDT further, another reconstruction using the same algorithm is performed with an independent data set using the smaller resolution test chart numbered A5, as shown in Fig. 8. Fig. 8(a) and (b) present the left and right low resolution sub-aperture images, respectively.

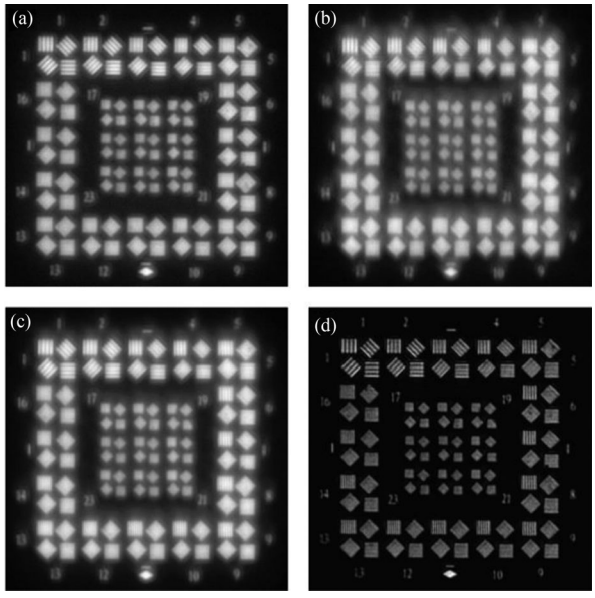

Fig. 8. Imaging results and reconstruction with the A5 resolution test chart. (a) The image formed by the single left aperture; (b) the image formed by the single right aperture; (c) the synthetic image formed by the co-phased two aperture; (d) the reconstructed image using SMDT.

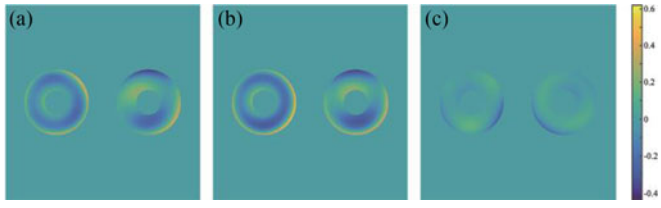

Fig. 9. Reconstructed two sub-aperture wavefronts using the data set of the (a) A4 and (b) A5 resolution test chart; (c) difference between (a) and (b).

The synthetic image is shown in Fig. 8(c), which seems to have higher resolution but suffers from seriously low contrast and blurring. Luckily, after using SMDT, we obtain a sharp image with quality and contrast obviously improved shown as Fig. 8(d). Additionally, from this set of experiment, we can see the practical resolution of our binocular testbed. As Fig. 8(d) shows, the spacing of the vertical bars of group 17 is the smallest distance we can resolve, corresponding to a spot angle of 2.65 μrad (the bar width is 3.97 um), which matches the horizontal theoretical resolution as analyzed in Section 2.

Finally, we compare this couple of wavefronts extracted from the two independent data sets, regarded as the reference of each other. Though a comparison with an independent measurement technique could definitely verify the accuracy, a repeating measurement error also helps indicate if we acquire accurate wavefront recovery, as introduced and used in Ref. [19]. The two repetitive wavefronts of the binocular telescope generated by two separated data sets of the A4 and A5 resolution test chart are shown as Fig. 9(a) and (b), respectively. Fig. 9(c) shows the difference between them, with a RMS error of 0.0638 waves. The good repeatability indirectly demonstrates the validity of SMDT for wavefront sensing in real sparse aperture systems.

5. Conclusion

In conclusion, we have demonstrated SMDT for image restoration in the binocular telescope system. The optical configuration of the testbed is described in detail and a directly synthetic image

is presented with horizontal resolution enhanced. However, the quality of the raw sparse aperture image is poor due to the blurring and loss of contrast. Then we develop an improved algorithm of SMDT by considering the sub-aperture aberrations independently for an actual sparse aperture system. Besides the synthetic image, other two diversity images are captured by switching off the electronic shutter in proper order. Based on the raw dataset, our improved algorithm is employed to recover the contrast and remove the blurring. The result that the recovered image shows enhanced sharpness and contrast with respect to the poor raw image verifies the effectiveness of our proposed method in image restoration of actual sparse aperture systems. For a more convincing demonstration, we additionally performed another reconstruction based on an independent data set using a smaller resolution test chart. The recovered image also shows great improvement in quality and contrast. As a check on the reconstructed wavefront, a comparison between the second result and the earlier one is given, showing a good repeatability.

Without requirement of other optics and multiple separate image planes, it is attractive and promising that SMDT uses simple and common electronic shutters to realize aberration sensing and image restoration. It has been demonstrated in a mask-pupil experiment and in this paper we have further demonstrated its validity for image restoration in an actual aperture system. After this demonstration, we believe SMDT can contribute to the existing multi-aperture system projects, such as the Large Binocular Telescope [28] and Star-9 [15], or other future ones.

Except for deconvolution, there are also other image processing techniques that can improve image quality, such as the feature point matching algorithm [29]. As for sparse aperture images, it shows potential to superpose sub-images, but the problem that the PSF is an interference pattern rather than an Airy disk might be a limitation. If this algorithm was improved with further study and could work for multi-aperture systems, though superposing sub-images (equivalent to correcting tip-tilt), it couldn't remove the aberrations and improve the contrast compared with our method.

We also note that here SMDT is used in a two-aperture system as an example, but of course it can be expanded for more apertures. When applied to an n-aperture system, SMDT needs to choose proper combinations of spatial modulations among 2^n-1 possibilities. There may be an optimal combination or some selection rules, which needs further study. However, with more sub-apertures, the times of spatial modulation SMDT needs also increase, causing more time expense. Therefore, some fast spatial modulation devices such as digital mirror device are required for SMDT applied to more apertures.

References

[1] S. Fender, "Synthetic apertures: An overview," *Proc. SPIE*, San Diego, CA, USA, vol. 440, pp. 2–7, Aug. 1983.

[2] J. R. Fienup, D. Griffith, L. Harrington, A. M. Kowalczyk, J. J. Miller, and A. A. Mooney, "Comparison of reconstruction algorithms for images from sparse-aperture systems," *Proc. SPIE*, Seattle, WA, USA, no. 4792, pp. 1–8, Jul. 2002.

[3] D. J. Rabb, D. F. Jameson, J. W. Stafford, and A. J. Stokes, "Multi-transmitter aperture synthesis," *Opt. Express*, vol. 18, no. 24, pp. 24937–24945, Nov. 2010.

[4] J. Stokes, B. D. Duncan, and M. P. Dierking, "Improving mid-frequency contrast in sparse aperture optical imaging systems based upon the Golay-9 array," *Opt. Express*, vol. 18, no. 5, pp. 4417–4427, Feb. 2010.

[5] C. J. Schuler, M. Hirsch, S. Harmeling, and B. Scholkopf, "Blind correction of optical aberrations," in *European Conference on Computer Vision*. New York, NY, USA: Springer, 2012, pp. 187–200.

[6] M. Figueiredo and R. Nowak, "An EM algorithm for wavelet-based image restoration," *IEEE Trans. Image Process.*, vol. 12, no. 8, pp. 906–916, Aug. 2003.

[7] Z. Zhou, D. Wang, and Y. Wang, "Effect of noise on the performance of image restoration in an optical sparse aperture system," *J. Opt.*, vol. 13, Jun. 2011, Art. no. 075502.

[8] W. Xu, M. Zhao, and H. Li, "Non-iterative wavelet-based deconvolution for sparse aperture system," *Opt. Commun.*, vol. 295, pp. 36–44, Jan. 2013.

[9] N. J. Miller, M. P. Dierking, and B. D. Duncan, "Optical sparse aperture imaging," *Appl. Opt.*, vol. 46, no. 23, pp. 5933–5943, Aug. 2007.

[10] R. A. Gonsalves, "Phase retrieval and diversity in adaptive optics," *Opt. Eng.*, vol. 21, no. 5, Oct. 1982, Art. no. 215829.

[11] R. G. Paxman and J. R. Fienup, "Optical misalignment sensing and image reconstruction using phase diversity," *J. Opt. Soc. Amer. A*, vol. 5, no. 6, pp. 914–923, Jun. 1988.

[12] R. G. Paxman, T. J. Schulz, and J. R. Fienup, "Joint estimation of object and aberrations by using phase diversity," *J. Opt. Soc. Amer. A*, vol. 9, no. 7, pp. 1072–1085, Jul. 1992.

[13] Z. Xie *et al.*, "Restoration of degraded images using pupil-size diversity technology with stochastic parallel gradient descent algorithm," *IEEE Photon. J.*, vol. 8, no. 2, Apr. 2016, Art. no. 6900410.

[14] Z. Xie *et al.*, "Wavefront sensing and image restoration with spatially overlapping diversity technology," *IEEE Photon. Technol. Lett.*, vol. 28, no. 17, pp. 1882–1885, Sep. 2016.
[15] R. L. Kendrick *et al.*, "Wide-field Fizeau imaging telescope: Experimental results," *Appl. Opt.*, vol. 45, no. 18, pp. 4235–4240, Jun. 2006.
[16] D. Mourard *et al.*, "Chromatic phase diversity for cophasing large array of telescopes," *Proc. SPIE*, Amsterdam, The Netherlands, vol. 8445, Sep. 2012, Art. no. 84451M.
[17] M. R. Bolcar and J. R. Fienup, "Sub-aperture piston phase diversity for segmented and multi-aperture systems," *Appl. Opt.*, vol. 48, no. 1, pp. A5–A12, Jan. 2009.
[18] H. Ma *et al.*, "Synthetic aperture imaging by using spatial modulation diversity technology with stochastic parallel gradient descent algorithm," *Opt. Express*, vol. 23, no. 11, pp. 14836–14849, Jun. 2015.
[19] G. R. Brady, M. Guizar-Sicairos, and J. R. Fienup, "Optical wavefront measurement using phase retrieval with transverse translation diversity," *Opt. Express*, vol. 17, no. 2, pp. 624–639, Jan. 2009.
[20] W. A. Traub, "Combining beams from separated telescopes," *Appl. Opt.*, vol. 25, no. 4, pp. 528–532, Feb. 1986.
[21] D. G. Voelz, "Imaging and diffraction-limited imaging simulation," in *Computational Fourier Optics*. Bellingham, WA, USA: SPIE, 2011, pp. 113–139.
[22] I. Paykin, L. Yacobi, J. Adler, and E. N. Ribak, "Phasing a segmented telescope," *Phys. Rev. E*, vol. 91, Feb. 2015, Art. no. 023302.
[23] X. He, H. Ma, and C. Luo, "Simulation of co-phase error correction of optical multi-aperture imaging system based on stochastic parallel gradient decent algorithm," *Proc. SPIE*, Suzhou, China, vol. 9682, Apr. 2016, Art. no. 96820V.
[24] R. A. Muller and A. Buffington, "Real-time correction of atmospherically degraded telescope images through image sharpening," *J. Opt. Soc. Amer.*, vol. 64, pp. 1200–1210, Sep. 1974.
[25] M. A. Vorontsov and V. P. Sivokon, "Stochastic-parallel-gradient-descent technique for high-resolution wave-front phase-distortion correction," *J. Opt. Soc. Amer. A*, vol. 15, no. 10, pp. 2745–2758, Oct. 1998.
[26] S. T. Thurman and J. R. Fienup, "Noise histogram regularization for iterative image reconstruction algorithms," *J. Opt. Soc. Amer. A*, vol. 24, no. 3, pp. 608–617, Feb. 2007.
[27] M. R. Bolcar, "Phase diversity for segmented and multi-aperture systems," *Ph.D. dissertation*, University of Rochester, Rochester, NY, USA, 2008.
[28] J. M. Hill, "The large binocular telescope," *Appl. Opt.*, vol. 49, no. 16, pp. D115–D122, Jun. 2010.
[29] J. Li, "An image feature point matching algorithm based on fixed scale feature transformation," *Optik*, vol. 124, no. 13, pp. 1620–1623, May 2013.